J Fluoresc (2012) 22:931–944
DOI 10.1007/s10895-011-1032-y

ORIGINAL PAPER

PEG Coated Biocompatible Cadmium Chalcogenide Quantum Dots for Targeted Imaging of Cancer Cells

Aby Cheruvathoor Poulose · Srivani Veeranarayanan · M. Sheikh Mohamed · Sreejith Raveendran · Yutaka Nagaoka · Yasuhiko Yoshida · Toru Maekawa · D. Sakthi Kumar

Received: 20 October 2011 / Accepted: 28 December 2011 / Published online: 8 January 2012

Abstract Cancer stands as a leading cause of mortality worldwide and diagnostics of cancer still faces drawbacks. Optical imaging of cancer would allow early diagnosis, evaluation of disease progression and therapy efficiency. To that aim, we have developed highly biocompatible PEG functionalized cadmium chalcogenide based three differently luminescent quantum dots (QDs) (CdS, CdSe and CdTe). Folate targeting scheme was utilized for targeting cancer cell line, MCF-7. We demonstrate the biocompatibility, specificity and efficiency of our nanotool in detection of cancer cells sparing normal cell lines with retained fluorescence of functionalized QDs as parental counterpart. This is the first time report of utilizing three differently fluorescent QDs and we have detailed about the internalization of these materials and time dependent saturation of targeting schemes. We present here the success of utilizing our biocompatible imaging tool for early diagnosis of cancer.

Keywords Cadmium chalcogenide QDs · PEG biofunctionalization · Cancer imaging · Folate targeting · Diagnostic tool

Introduction

Cancer has become a very common multifactorial disease and cause of leading mortality worldwide [1, 2]. Increasing incidence of cancer worldwide demands advancements for early diagnostics and for monitoring treatment regimens and their outcomes. X-ray computed tomography (CT) and Magnetic resonance imaging (MRI) are the current available imaging techniques capable of identifying tumors anatomically [3]. However the sensitivity of these techniques is not upto the mark at molecular level, limiting its potential application in early cancer diagnostics [4]. Cancer nanotechnology has become a well researched interdisciplinary field enabling fabrication of nanotools to yield high image contrast, sensitivity and specificity [5–7]. Recent research has witnessed wide range of fluorescent nanomaterials applied for biological imaging [8]. Fluorescent markers at single molecular level are the need of the hour in particular for imaging molecular events inside live cells, such as signaling pathways for the study of cellular metabolism [9–14]. Fluorescent nanoparticle based cancer imaging probes has been researched and processes like synthesis, surface modification and bioconjugation of nanotools for specificity in cancer targeting are now well documented [15, 16]. Semiconductor quantum dots need special mention as imaging tools because of their unique properties of bright photostable nature. They possess size and composition adjustable fluorescence emission wavelengths with broad absorption spectrum and narrow emission spectrum [17–20]. Fluorescent QDs could be developed in typical size range of 2–10 nm consisting of elements primarily from groups II and VI and groups III and V in the periodic table. These QDs show spectral emission order of magnitude higher than conventional fluorophores. The surfaces of quantum dots are easily available for surface modification [21].

QDs are usually synthesized by hot injection organometallic route which makes them hydrophobic and are not readily water soluble [22]. To make them water soluble time consuming labor intensive coating methodologies are to be

A. Cheruvathoor Poulose · S. Veeranarayanan · M. S. Mohamed · S. Raveendran · Y. Nagaoka · Y. Yoshida · T. Maekawa · D. S. Kumar (✉)
Bio Nano Electronics Research Center, Graduate School of Interdisciplinary New Science, Toyo University, Kawagoe, Saitama 350-8585, Japan
e-mail: sakthi@toyo.jp

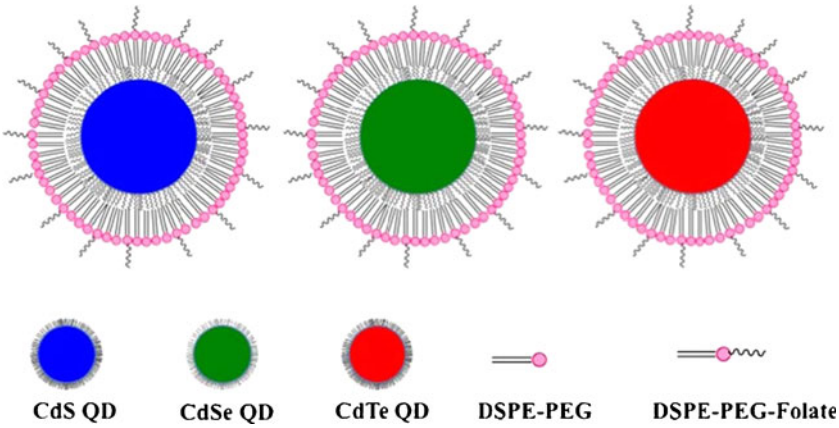

Fig. 1 Schematic representation of PEG-Bio-functionalized QDs

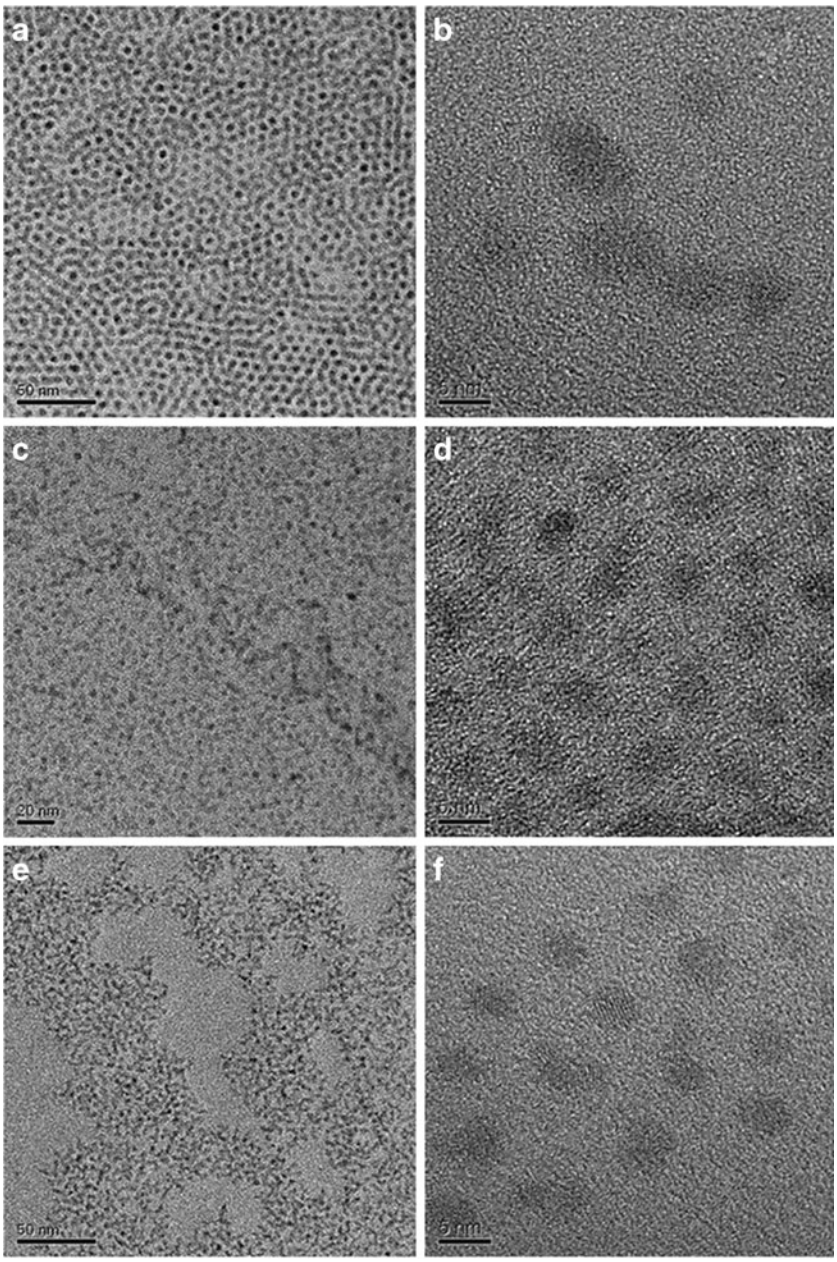

Fig. 2 TEM images of bare cadmium chalcogenide QDs. **a** TEM image of CdS QD. **b** HRTEM of CdS QD. **c** TEM image of CdSe QD. **d** HRTEM of CdSe QD. **e** TEM image of CdTe QD. **f** HRTEM of CdTe QD

carried out. In addition, the coating methodologies can lead to high toxicity, as in case of mercaptopropionic acid (MPA) coated QDs. MPA is itself toxic and coating with them to make water soluble will not help in biological applications. Water soluble coating of QDs can also lead to reduction in photostability of QDs and can decrease the luminescent intensity when compared to the bare ones [23]. For application in biology, we are in need of excellent biocompatible highly specific QDs, which should not render any cytotoxicity to cells and are highly specific to their targets sparing normal cells [24]. In cancer diagnostics, high specific targeting and sensitivity are necessary to make these nanotools as efficient diagnostic system when compared to available CT and MRI systems.

To make QDs water soluble, hydrophilic surface coating of QDs is necessary. PEG is considered to be best biocompatible material which is widely used to make nanotools cyto-amaiable [25]. Lipids conjugated with PEG moieties can be successfully utilized for preparation of highly biocompatible QDs without any loss in fluorescene intensity of the QDs. Lipids and liposomal components are approved by FDA and are already in formulations used in various theragnostic regimens. Liposomal formulations possess hydrophilic surface which are considered to be efficiently taken up or internalized by live cells. In addition PEG-Lipid conjugates are available for extensive surface modification and biofunctionalization due to their highly reactive functional groups aiding in conjugation of antibodies, aptamers, peptides etc.. for targeting cancer cells with high specificity [26, 27]. The preparation of QD Lipid-PEG conjugates has been accomplished by encapsulating the hydrophobic core within the aqueous lipid core with hydrophilic PEG moieties branching exterior by film hydration process [28]. Especially PEG-DSPE moieties when coated onto nanomaterials are known to increase the circulation time of nanotools by decreasing the clearance by reticulo endothelial system [29, 30].

Our objective is to utilize cadmium based QDs for effective imaging of tumor. Cadmium based QDs show excellent luminescent properties but they are highly toxic due to release of toxic cadmium ions. Here we report preparation of highly biocompatible PEG-DSPE coated cadmium chalcogenide QDs (CdS, CdSe and CdTe) of blue, green and red luminescence and application of them in cancer cell imaging by folate targeting scheme. We are able to image cancer cells with high specificity by sparing normal cells and we could enhance the biocompatibility of these coated nanomaterials in normal cells. The biocompatibility of cadmium based QDs increased by nearly 60% in case of PEG coating. This is the first time report of utilizing three differently luminescent cadmium based QDs and the reported biocompatibility achieved as high as 90% for PEG-Lipid coated QDs without any passivating shell.

Experimental Section

Preparation of Cadmium Precursor for QD Synthesis

Cadmium chalcogenide QDs (CdS, CdSe and CdTe) were prepared by conventional organometallic route. Cadmium oxide was used as cadmium precursor and Sulfur, Se and Te powder were used as chalcogenide precursors respectively.

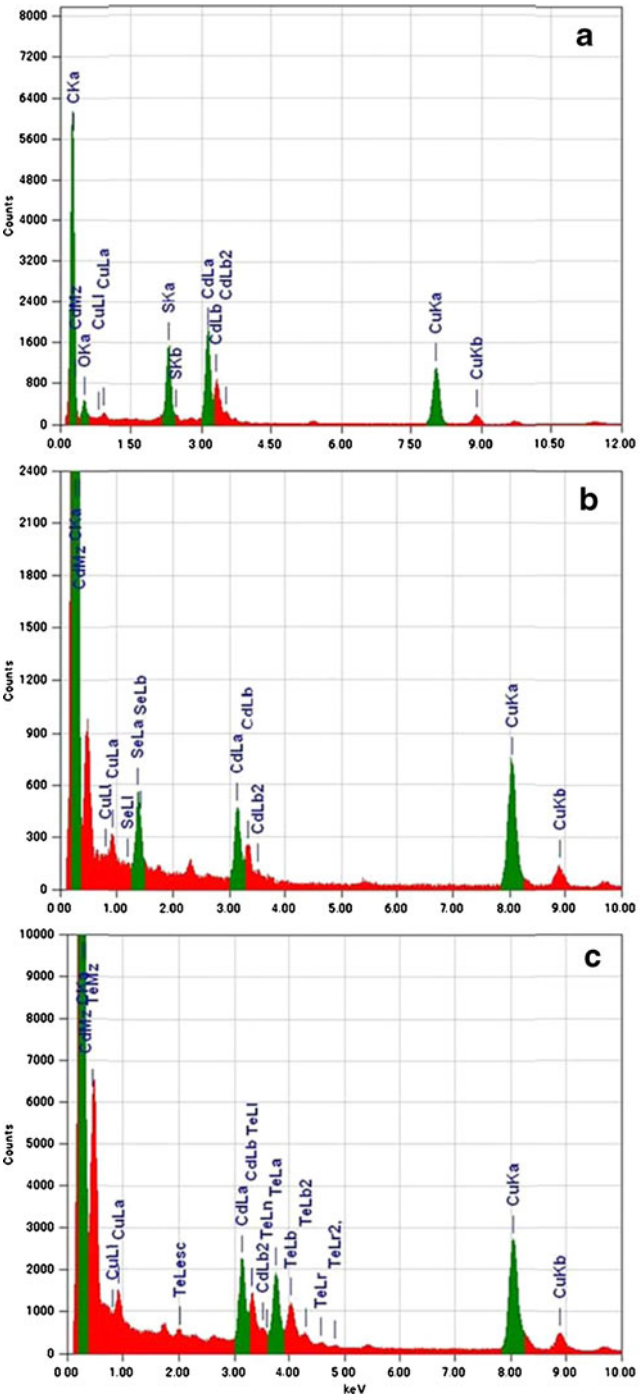

Fig. 3 EDS analysis of bare cadmium chalcogenide QDs. Elemental analysis of CdS (**a**), CdSe (**b**) and CdTe (**c**)

0.01 mmole of Cadmium oxide was dissolved in octadecene (10 ml), a noncoordinating solvent in the presence of oleic acid (0.6 ml), as capping agent. The solution was heated to 200 °C under Argon atmosphere until the solution becomes transparent.

Synthesis of CdS QDs

Sulfur precursor was prepared by adding 0.05 mmole of Sulfur powder to 5 ml of octadecene. The solution was stirred vigorously and heated to dissolve the sulfur powder completely. The above prepared cadmium precursor was heated to 300 °C and the 1 ml sulfur precursor kept at room temperature was injected rapidly and the resulted solution was cooled down to 260 °C and allowed the reaction to carry out for 1 min. Transparent bright yellow color appeared after reaction for 1 min which indicates the formation of CdS QDs.

Synthesis of CdSe QDs

0.05 mmole of Selenium powder was dissolved in octadecene and tri-n-octylphosphine (TOP) by heating the solution until a clear suspension is obtained. Cadmium precursor solution was heated to 225 °C and room temperature 1 ml selenium precursor solution kept at room temperature was quickly injected in it to initiate the reaction. The temperature of the solution was decreased to 220 °C upon injection of selenium precursor and the reaction was prolonged for 1 min to yield CdSe QDs.

Synthesis of CdTe QDs

Tellurium powder was dissolved in octadecene and tributylphosphine (TBP) and the solution was stirred and heated vigorously to yield clear solution of Te precursor. Cadmium precursor was heated to 180 °C and 1 ml tellurium precursor solution kept at room temperature was injected to it. The solution was cooled to room temperature immediately to quench the reaction because CdTe formation was quite rapid.

Table 1 Zeta potential and hydrodynamic diameter of bare and PEG bio-functionalized QDs

Type of QD	Zeta Potential (mV)		Hydrodynamic diameter (nm)	
	Bare QD	Bio-functionalized QD	Bare QD	Bio-functionalized QD
CdS QD	1.97	−8.59	7	232
CdSe QD	0.785	−2.77	4	179
CdTe QD	−0.637	−9.94	5	208

Biofunctionalization of QDs

The schematic representations of PEG-Bio-functionalized QDs are shown in Fig. 1. Oleic acid capped cadmium chalcogenide QDs prepared by above procedures were

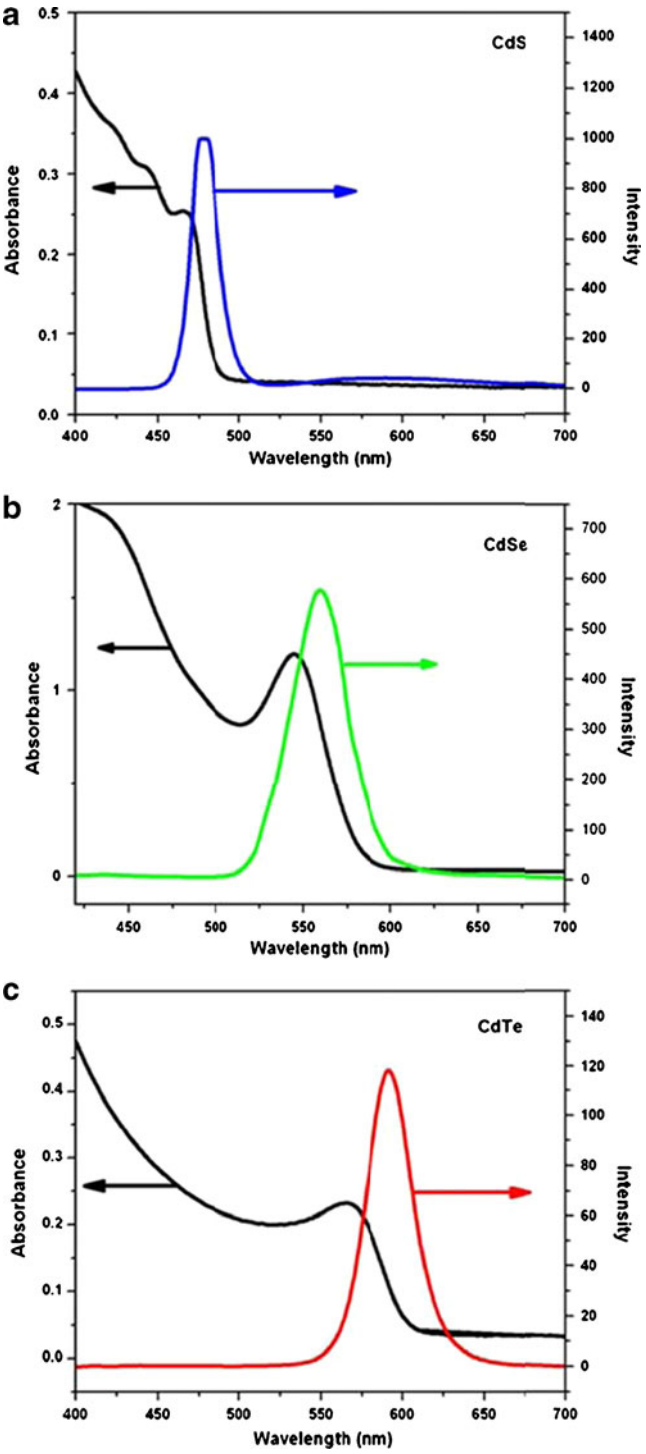

Fig. 4 Absorption and PL spectra of bare and cadmium chalcogenide QDs. **a** CdS, **b** CdSe and **c** CdTe. In the case of PL spectra we have used an excitation wavelength of 365 nm

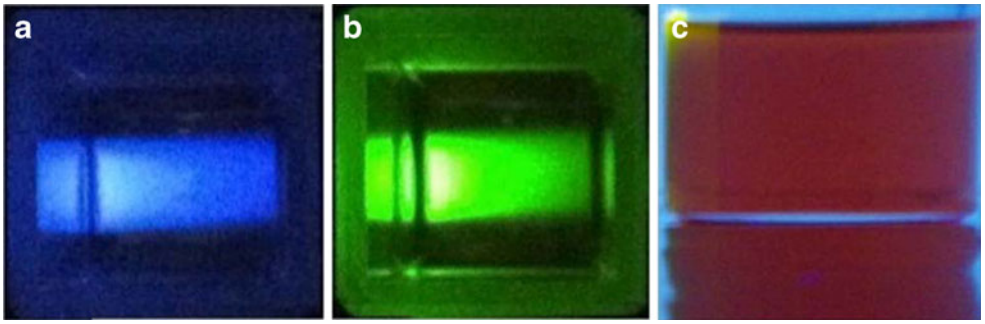

Fig. 5 UV light (365 nm) illumination of bare CdS (**a**), CdSe (**b**) and CdTe (**c**) QDs

utilized for biofunctionalization. Thus prepared QDs were precipitated with ethanol thrice and the final product was dispersed in 10 ml chloroform. Maleiimide-PEG and Folate conjugated PEG (PEG-Fol) dispersed in chloroform and methanol was used for bioconjugation. 1 ml of QD suspension (dispersed in chloroform) was taken and Maleiimide-PEG (PEG-Mal) and PEG-Fol were added to the QD suspension and the solvent was gently evaporated completely to yield thin film of QDs and PEG. This thin film was then hydrated with 70 °C HEPES buffer of pH 6.7 and the suspension was stirred and heated vigorously to yield clear aqueous suspension of QDs functionalized with PEG moieties. Empty micelles of PEG were completely removed by ultra-centrifugation yielding biofunctionalized QDs.

Materials for Biological Studies

MCF-7 and L929 cell lines were obtained from Riken bioresources, Japan. Trypan blue, 0.025% Trypsin were purchased from Sigma-Aldrich. Alamar blue toxicology kit, DAPI and Lysotracker was purchased from Invitrogen.

Cell Culture Maintenance

MCF-7 and L929 cell lines were maintained in T25 flasks using DMEM medium supplemented with 10% FBS and antibiotics (100 U/ml penicillin and streptomycin). The cells were sub-cultured every 2 days. The cells were maintained in glass base dish for confocal studies and plated in six well plates for biocompatibility phase contrast study and in 96 well plates for cytotoxicity studies.

Particle Characterization Studies

The morphology of cadmium chalcogenide QDs were studied with Field Emission Transmission Electron Micrograph, TEM (JEM-2200-FS). The prepared nanocrystals was analysed under TEM to obtain fine structure of QDs and lattices of the crystals. The UV–vis absorption and Photoluminescence (PL) spectra of bare and functionalized QDs were studied using Shimadzu UV-2100PC/3100PC UV visible spectrometer and Jasco FP750 spectrofluorometer. In the case of bare QDs, the suspension was diluted using chloroform and subjected for absorption and PL analysis. For functionalized QDs, HEPES buffer was used as solvent. The QD suspension was illuminated using UV light (365 nm) and its fluorescence was captured via Pentax Optio W80 digital camera. Dynamic light scattering (Malvern Zetasizer Nano-ZS) was employed to analyze the size of these nanomaterials (Bare QDs and functionalized QDs) in dispersion and their dispersive nature was also studied after they were dissolved in their respective solvents, chloroform in case of bare QDs and HEPES buffer in case of functionalized QDs. Zeta potential of as synthesized bare QDs and biofunctionalized QDs were also carried out. EDS (JEOL JED-2300T) was carried out to analyze the elemental composition of bare and functionalized QDs. FT-IR spectrum was recorded for bare and bifunctionalized QDs by Spectrum 100 FT-IR Spectrometer connected with Universal ATR Sampling Accessory (Perkin Elmer). The samples in their respective solvents were dropped on to the ATR crystal and spectra were recorded.

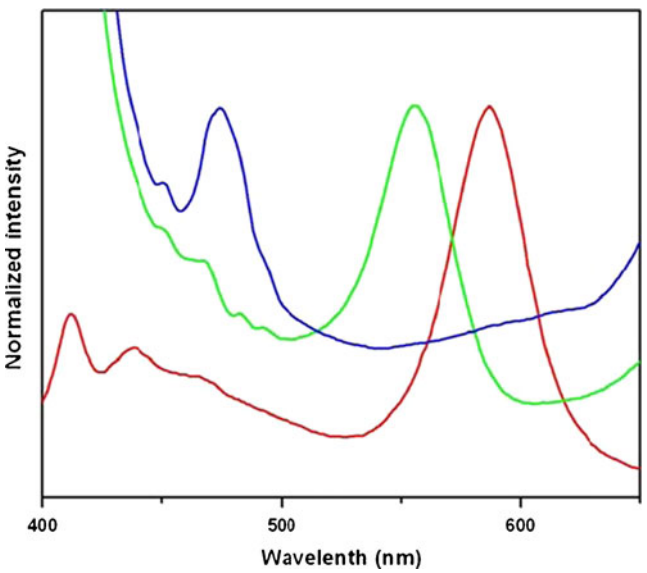

Fig. 6 PL spectra of PEG bio-functionalized QDs showing folate emission peak along with respective QD peak. The *blue*, *green* and *red lines* represents CdS, CdSe and CdTe at 365 nm excitation respectively

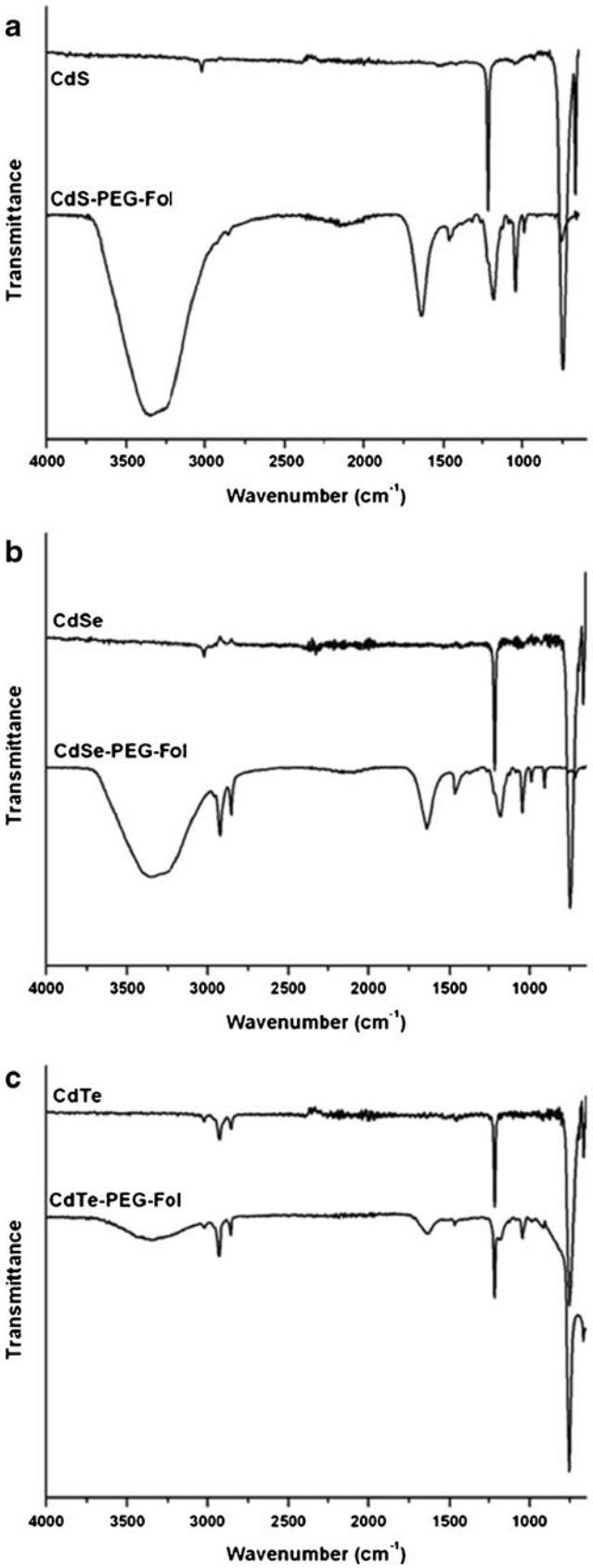

Fig. 7 FT-IR spectra of bare and PEG functionalized QDs. FT-IR spectra of CdS (**a**), CdSe (**b**) and CdTe (**c**)

Measuring the Cytotoxicity of Bare and Biofunctionalized QDs

The cytotoxicity of bare QDs and PEG functionalized QDs were studied in MCF-7 and L929 cell lines using alamar blue assay on 96 well plates. Alamar blue assay indicate about the reduction ability of the cells denoting the active metabolism occurring inside the cell. This active metabolism reduces when the test materials show toxicity leading to reduced reduction capability. The fluorescence intensity of alamar blue assay was quantified at 580–610 nm. 5,000–7,000 MCF-7 and L929 cells were plated respectively and were grown for 24 h or until visual confluency was noted. Two different concentrations (100 μl, 1X and 10 μl, 0.1X) of bare and biofunctionalized QDs dissolved in media were added and incubated for 24 h and assayed further. The experiment was conducted in triplicates and the viability

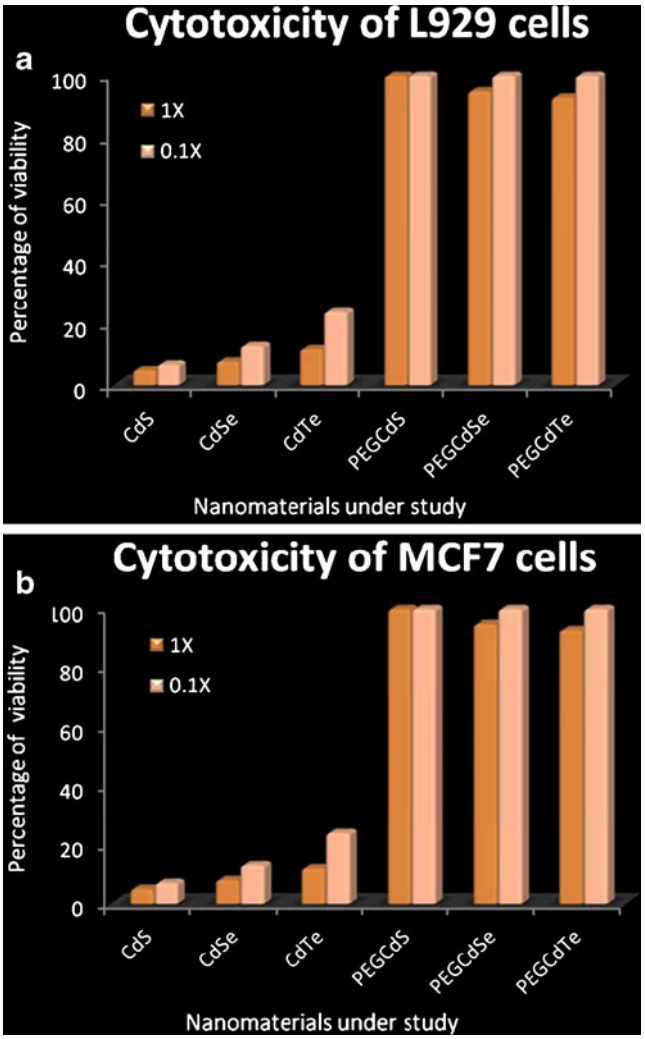

Fig. 8 **a** Cytotoxicity of bare and PEG-bio-functionalized QDs in normal, L929 cells. **b** Cytotoxicity of bare and PEG-bio-functionalized QDs in cancer cell line MCF7. (100 μl—1X and 10 μl—0.1X of as prepared QDs and biofunctionalized QDs were used)

was assessed using a microplate reader (Multidetection Microplate Scanner, Dainippon Sumitomo Pharma) by measuring the absorbance and fluorescence intensity of the resultant product.

Biocompatibility Test

MCF-7 and L929 cells were plated onto 6 well plates at a count of 50,000–60,000 cells per well. The cells were grown till visual confluency was reached and 1X concentration of bare QDs and bioconjugated QDs were added and the plates were incubated for 24 h. After 24 h, the cells were imaged using phase contrast microscopy (Nikon Eclipse TE2000-U with Nikon Intensilight C-HGFI) to note the biocompatibility of bare and conjugated QDs.

Confocal Microscopy

To visualize the uptake of QDs (bare and bioconjugated) by the cells, confocal microscopy was employed. Cells were grown on glass base dish for 24 h with standard medium and conjugated QDs was added at 1X concentration and were incubated for two different time scale, 2 h and 4 h. After 2 h, the nutrient medium was removed and the cells were washed with PBS buffer twice and stained with DAPI and lysotracker and were viewed under confocal microscopy (Olympus IX 81 under DU897 mode).

Results and Discussion

To prepare highly luminescent QDs, we have utilized hot injection organometallic route. The cadmium precursor and chalcogenide precursors were mixed and the suspension was maintained at ambient temperature to form CdS, CdSe and CdTe QDs. Thus synthesized CdS QDs show bright blue luminescent emission, CdSe was green luminescent and CdTe was bright red in luminescent emission. Synthesized QDs were subjected to biofunctionalization using PEG moieties (PEG-Mal and PEG-Fol) to render biocompatibility and specificity for these highly luminescent nanomaterials. As shown in TEM micrographs, the CdS QDs showed uniform size and shape with a diameter of 5 nm (Fig. 2a). The images also imply that the materials are highly monodisperse without any sign of particle aggregation. In the case of CdSe (Fig. 2c), the QDs were of uniform size of 3 nm in diameter and were highly monodisperse. CdTe QDs of 3 nm size in diameter was synthesized and showed high monodispersity and were of uniform spherical shape (Fig. 2e). The High resolution TEM images of CdS (Fig. 2b), CdSe (Fig. 2d) and CdTe (Fig. 2f) shows the sharp crystal lattices pattern of these cadmium chalcogenide QDs. EDS analyses were performed on bare QDs nanomaterials. EDS confirmed the presence of Cd and S (Fig. 3a), Cd and Se (Fig. 3b) and Cd and Te (Fig. 3c) in the case of CdS, CdSe and CdTe bare QDs respectively. To analyze the effect of biofunctionalization

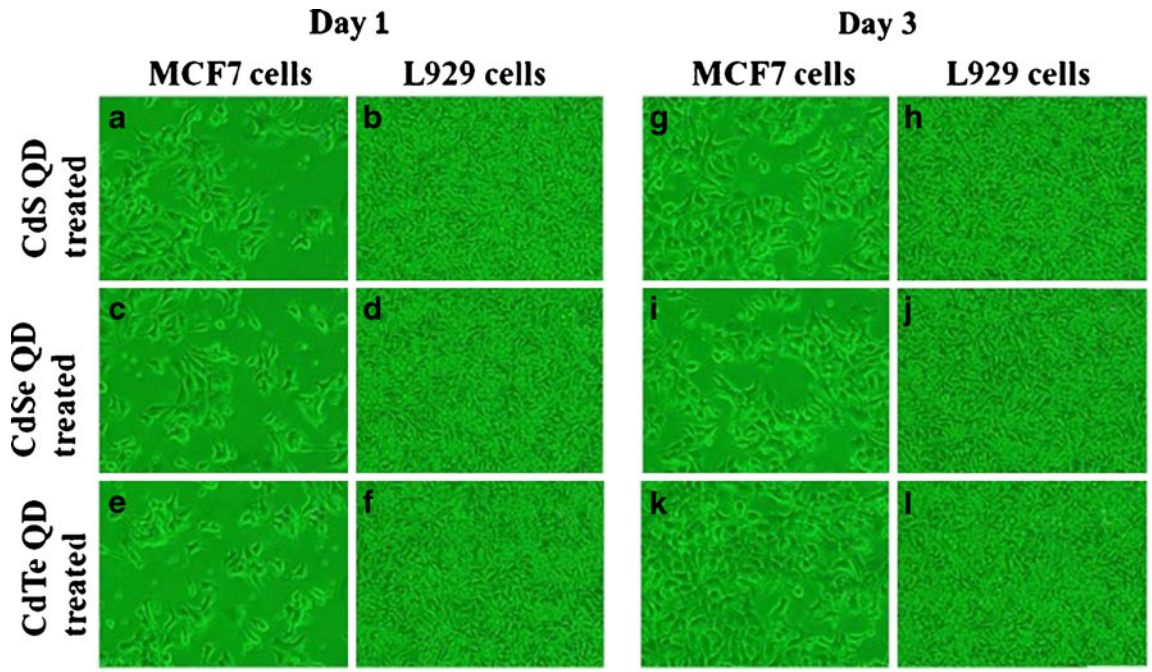

Fig. 9 Biocompatibility of normal and cancer cells treated with biofunctionalized QDs on day 1 and day 3. **a**, **b**, **c**, **d**, **e** and **f** are images showing biocompatibility of cells after 1 day of incubation. **g**, **h**, **i**, **j**, **k** and **l** are images showing biocompatibility of cells after 3 day of incubation. **a**, **b**, **g** and **h** are panel of cells treated with CdS, **c**, **d**, **i** and **j** are treated with CdSe and CdTe treated cells are shown in **e**, **f**, **k** and **l**

on the morphology of QDs, we carried out TEM analysis of functionalized QDs. The functionalized QDs were dispersed in HEPES buffer, added onto TEM grid and analyzed for coating over them (data not shown). We have observed increase in size of PEG functionalized QD mostly around 100–200 nm, proving the functionalization of PEG onto QDs. SEM analysis of PEG functionalized QDs also showed particles of size mostly 100–200 nm.

Dynamic light scattering (Zetasizer) was utilized to measure the size distribution of the bare (suspended in chloroform) and biofunctionalized QDs (suspended in HEPES buffer). The single peak obtained suggests uniform narrow size distribution and monodispersity of the bare QDs and broad distribution in case of functionalized ones. By DLS (Table 1), we observed the mean diameter of bare CdS, CdSe and CdTe QDs were 7 nm, 4 nm and 5 nm respectively, which supports the TEM analysis. We have observed an increase in size, in case of biofunctionalized QDs, a broad distribution peak ranging from 100 nm to 200 nm, which clearly shows the PEG functionalization and grafting over QDs to form a liposomal coating (data not shown) which were confirmed by SEM and TEM analysis.

To investigate the uniformity of the coupling of PEG moieties to QDs, we measured the zeta potential of the bare and biofunctionalized QDs. The Zeta potential measures the potential at the interface between a solid surface and the liquid medium. We observed a clear negative shift in zeta potential of biofunctionalized QDs when compared to the

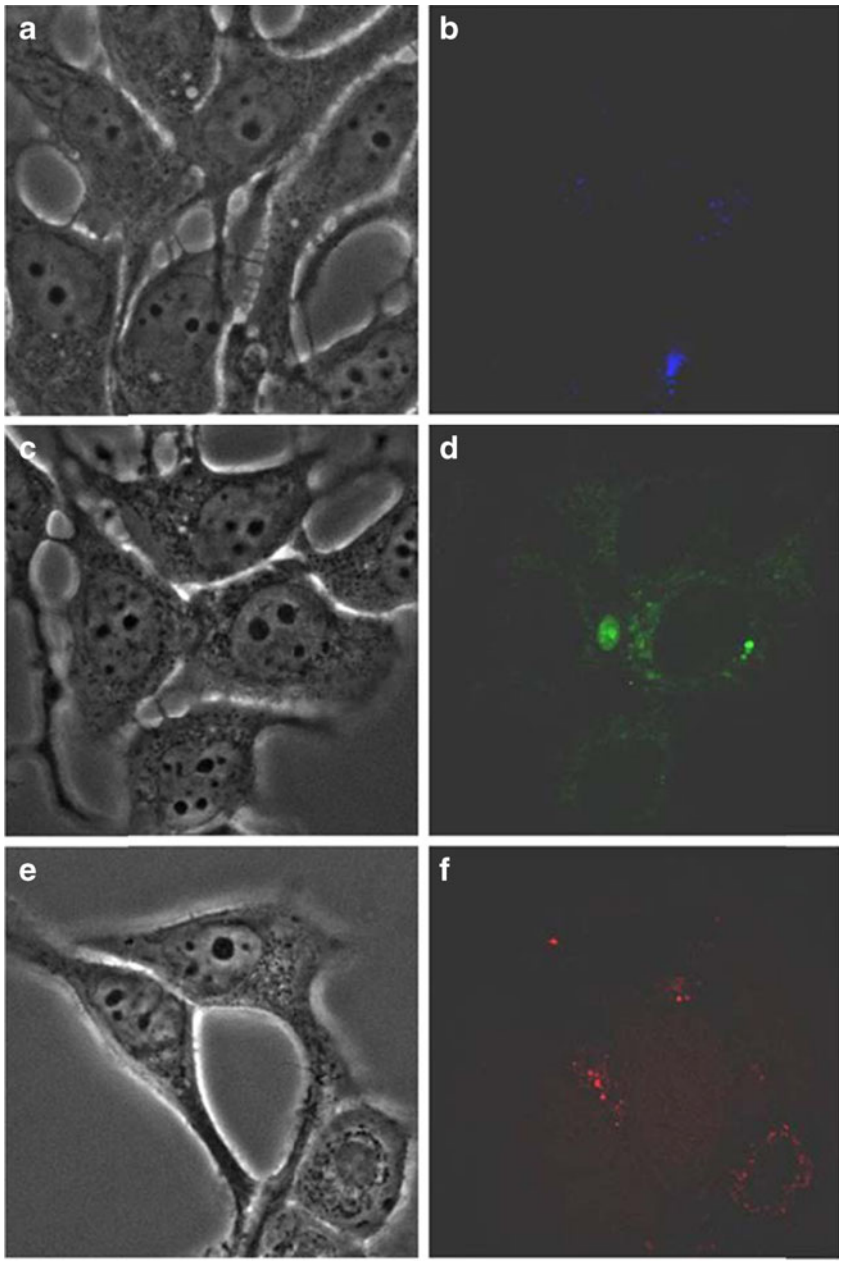

Fig. 10 Confocal image of MCF7 cells treated with bio-functionalized QDs. **a** and **b** CdS treated, **c** and **d** CdSe treated and e and f CdTe treated for 2 h

bare ones [31]. In case of CdS, we observed a zeta potential of +1.97 mV for bare ones and −8.59 mV for functionalized one. Bare CdSe showed a zeta potential of +0.785 and functionalized one showed a shift towards negative potential, −2.77 mV. CdTe bare and functionalized QDs showed a zeta potential of −0.637 mV and −9.94 mV. The above zeta potential shift (Table 1) towards negative potential for bio-functionalized QDs clearly proves the proper conjugation of PEG moieties onto bare QDs.

Figure 4a shows absorption and PL spectra of bare blue luminescent CdS QDs. The maximum absorption was seen around 450 nm and maximum emission was seen at 470 nm. In case of green luminescent CdSe QDs (Fig. 4b), the maximum absorption and emission was seen at 540 and 560 nm. The maximum absorption and emission of CdTe which was red luminescent was found to be 575 nm and 600 nm respectively (Fig. 4c). UV illumination of bare CdS, CdSe and CdTe QDs were shown in Fig. 5. The typical bright blue, green and red luminescence of bare cadmium chalcogenides was maximum and was captured using digital camera. The PL spectra of QD biofunctionalized PEG-Fol was shown in Fig. 6, which clearly shows the emission spectra of Folate, around 400 nm along with the emission spectra of respective QDs. This clearly shows the presence of PEG-Fol attached onto bare QDs elucidating the functionalization stands successful. The PL along with the DLS, Zeta potential and TEM image clearly shows the bioconjugation of PEG moieties onto the bare QDs.

FTIR spectra of unmodified and PEG functionalized QDs are shown in Fig. 8. The C–O–C ether stretch band around

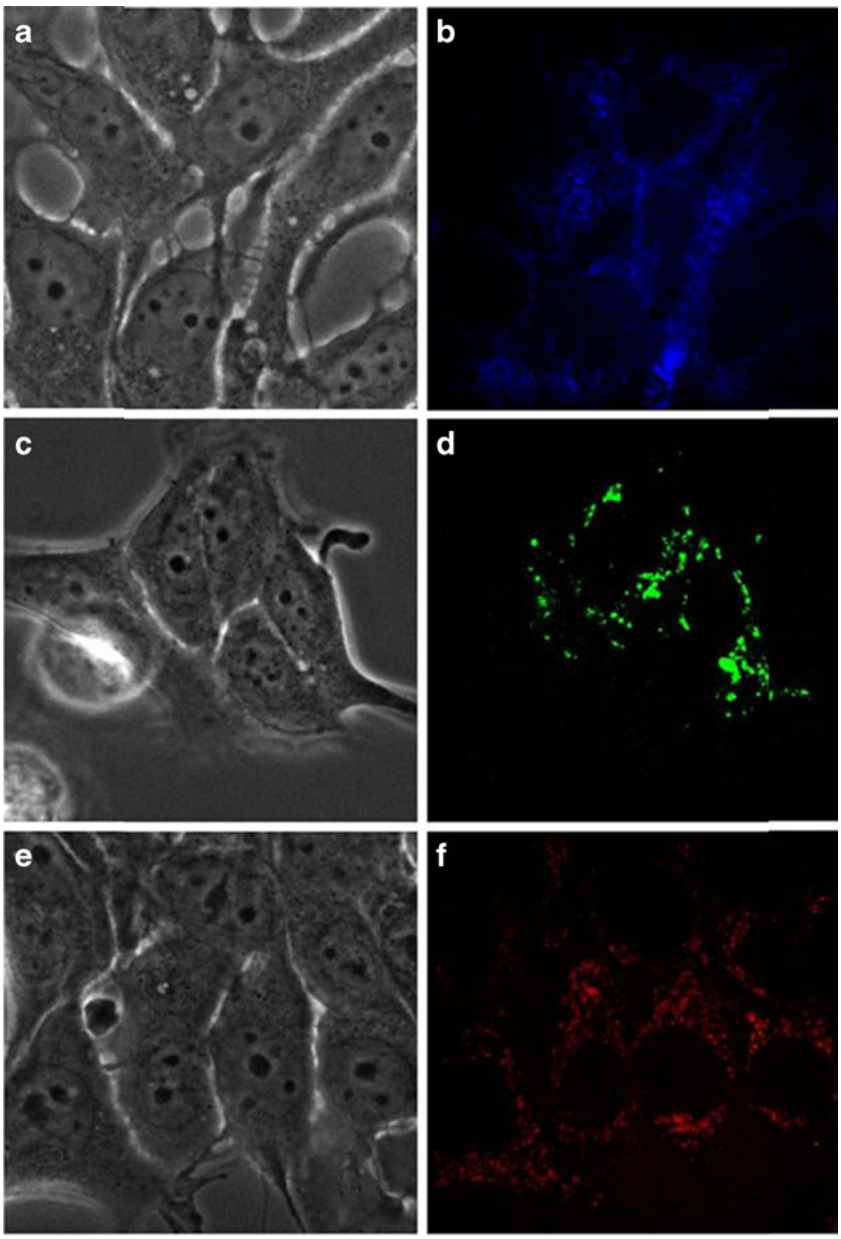

Fig. 11 Confocal image of MCF7 cells treated with bio-functionalized QDs. **a** and **b** CdS treated, **c** and **d** CdSe treated and **e** and **f** CdTe treated after 4 h incubation

1,175 cm^{-1} appear in the FTIR spectrum in case of all biofunctionalized QDs (CdS-Fig. 7a, CdSe-Fig.7b and CdTe-Fig. 7c) and are absent in bare QDs. Similarly, the bands around 2,918 and 981 cm^{-1} correspond to $–CH_2$ stretching vibrations and –CH out-of-plane bending vibrations, respectively. The characteristic IR absorption peaks of folate at 1,629 cm^{-1} were observed in the spectrum of PEG-Fol functionalized QDs. The C–O–C (strech), $–CH_2$(strech), –CH (bend) and folate (strech) peaks are strong evidence that PEG and PEG-Fol was bonded to the surface of QDs [32, 33].

Cytotoxicity profile of bare and biofunctionalized QDs were studied on L929, normal cell (Fig. 8a) and MCF-7 cancer cell line (Fig. 8b) grown on 96 well plate using Alamar blue assay. The nanomaterials of 100 μl and 10 μl of the crude sample prepared as such were added to the cells. We observed that cell viability decreased as a function of concentration and time. Alamar blue assay observed under two different concentrations after 24 h incubation with the nanomaterials. The cells showed uptake of nanomaterials within 2 h of incubation as evidenced from confocal studies and hence it is concluded that by 24 h the cytotoxic studies can be carried out. Bare QDs showed higher toxicity with only less than 20% cell viable with all QDs on average, even at the lowest concentration (0.1X) on both cell lines. We found that the cell viability was higher than 90% even at the highest concentration of 1X of bio-functionalized QDs highlighting the biocompatibility of

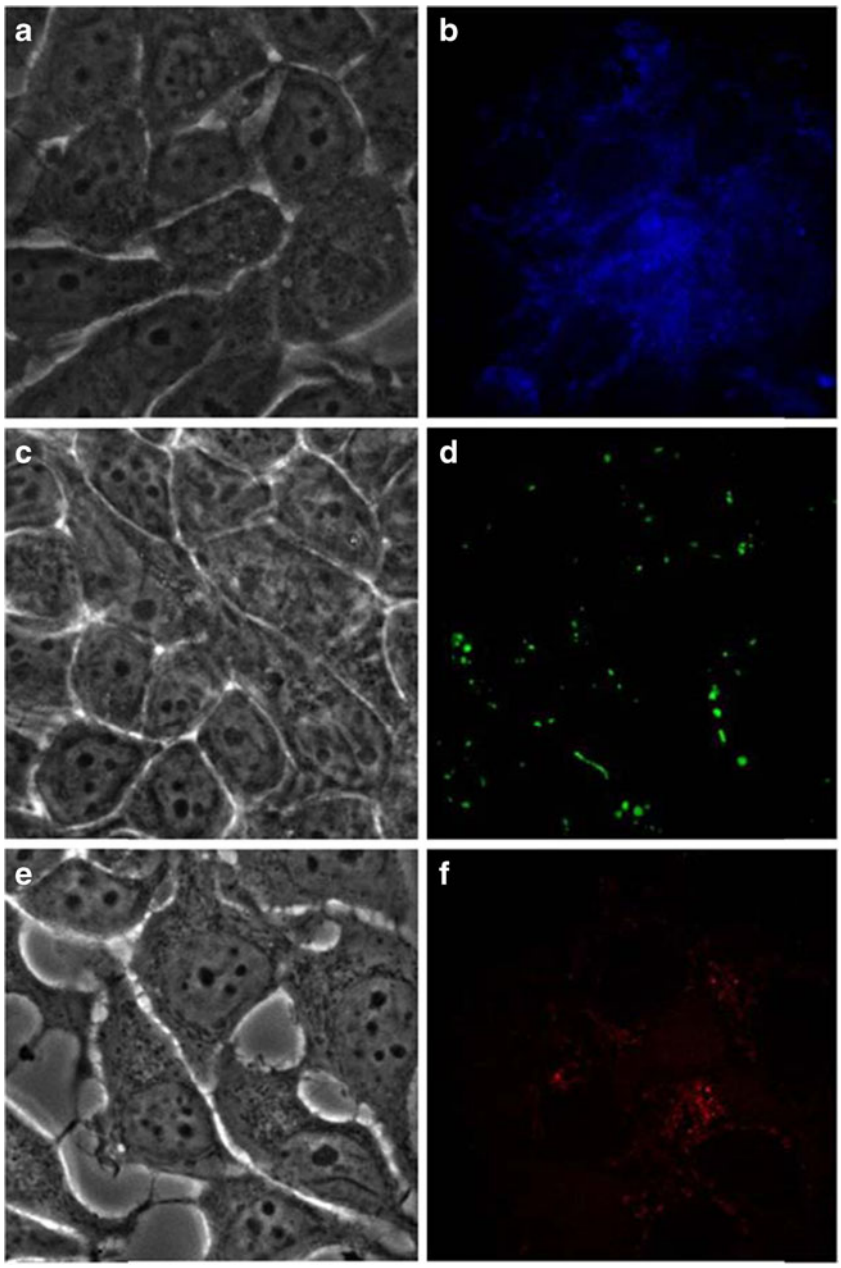

Fig. 12 Confocal image of MCF7 cells treated with bio-functionalized QDs. **a** and **b** CdS treated, **c** and **d** CdSe treated and **e** and **f** CdTe treated after incubating for 6 h

these nanomaterials on both cell lines studied. We observed same viability of cells even on day 2 (after 48 h incubation) and on day 3 (after 72 h incubation). These above biocompatibility results shows that QDs were encapsulated into liposomal shell of PEG moieties and release of cadmium ions was quenched to a great extent, thereby we could not observe any toxicity of biofunctionalized nanomaterials till day 3. This clearly shows that biofunctionalized QDs exert no significant cytotoxic effects on L929 cells and MCF-7 cells and thus present themselves as highly safe biocompatible labeling probes compared to bare QDs.

To analyze and visualize the biocompatibility of functionalized QDs, L929 cells and MCF-7 cells were grown on 6 well plates until visual confluency was achieved. 1X concentration of functionalized QDs was added to each well and the plates were incubated for 3 days. After every 24 h, the images were taken using phase contrast microscopy to show the biocompatibility of these QDs (Fig. 9a, b, c, d, e and f). We could not observe any cytotoxicity rendered by these QDs and the results showed that the cells were nearly 100% viable till day 3 (Fig. 9g, h, i, j, k and l). The phase contrast images shown in Fig. 9 clearly shows any deformity in size and shape of the cells and were growing competently on pace with the control cells.

Cellular uptake and endocytosis of biofunctionalized QDs were studied by confocal microscopy to determine

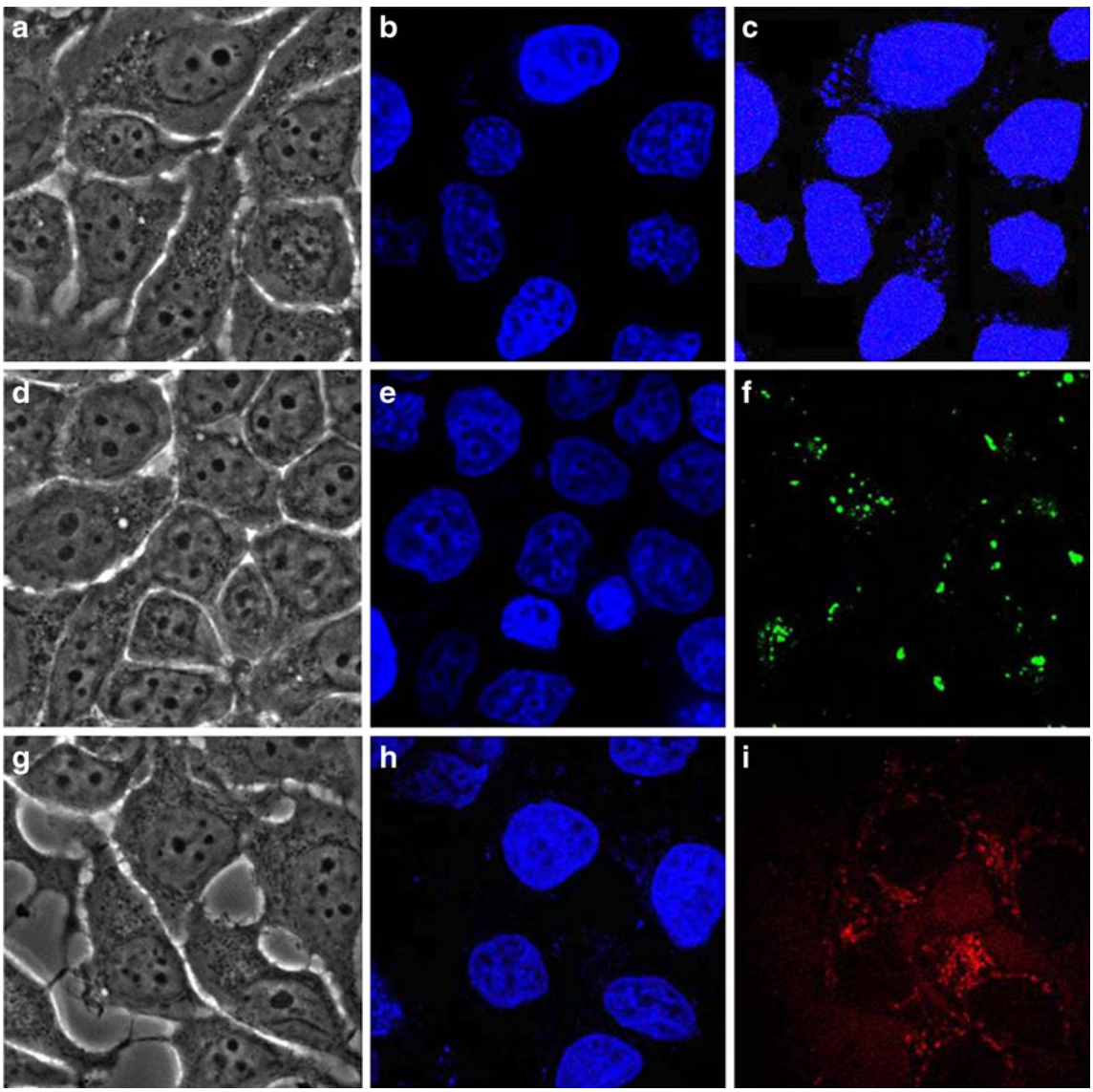

Fig. 13 DAPI staining of bio-functionalized QDs treated cells showing viable nucleus. **a**, **b** and **c** CdS treated cells, **d**, **e** and **f** CdSe treated cells and **g**, **h** and **i** CdTe treated cells after 4 h of particle incubation. The left panel shows the bright field image of MCF7 cells, the middle column shows the DAPI staining of cells and the right column shows fluorescent image of particle localized inside cells. In case of CdS treated cells, the fluorescent image and DAPI staining was observed using same excitation. We could observe particles internalized in the cell's cytoplasm clearly

the intracellular fate of these nanomaterials. Cells were treated with as low as 1X concentration of biofunctionalized QDs and incubated for different time scale (2 h, 4 h and 6 h) to study the time dependent uptake of these QDs in L929 and MCF-7 cells. L929 cells were used as negative control because they carry less number of folate receptors than their cancer counterpart, MCF-7. After 2 h, the cells were viewed under confocal microscopy (Fig. 10). In case of biofunctionalized CdS QDs, the excitation wavelength used for confocal studies was 405 nm. When excited, MCF-7 cells showed clear and discrete signal of blue luminescent CdS pinning their internalization into the cell (Fig. 10a and b). We observed discrete green luminescent CdSe (Fig. 10c and d) and red luminescent CdTe signals (Fig. 10e and f) when the respective plates were excited with wavelength of 488 nm and 561 nm respectively. We observed discrete luminescent signals of QDs from certain round vesicles inside the cell. To analyze whether lysosomal mediated entry of QDs existed, we used green fluorescent lysotracker for mapping the downstream internalization in case of biofunctionalized CdS and CdTe treated cells (data not shown). We observed lysosomal mediated endocytosis of these QDs as per previous literature [34].

After 4 h incubation, the second sets of cells were subjected for confocal studies. We observed increased internalization of particles inside MCF-7, which clearly depicts the

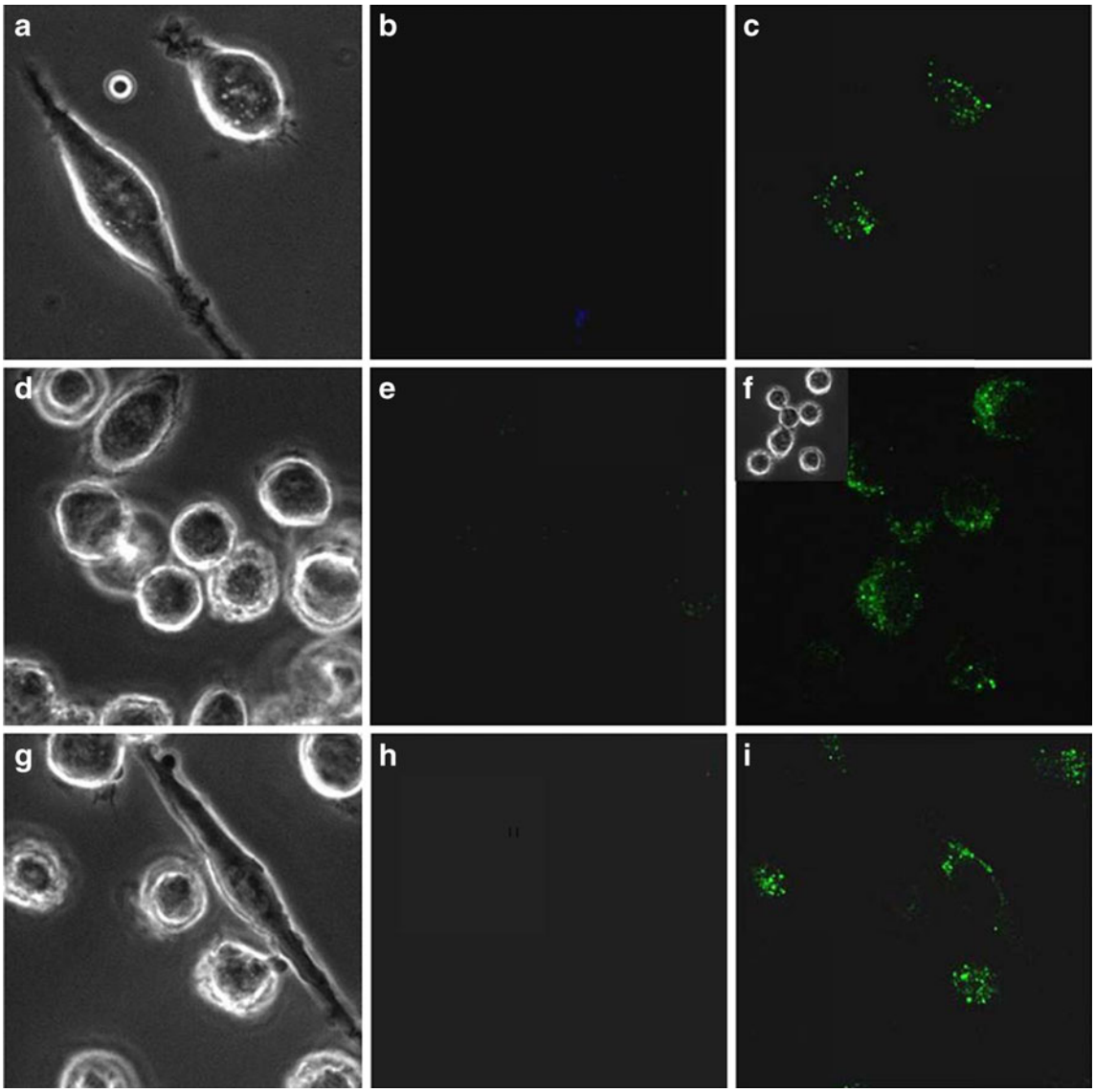

Fig. 14 Fluorescent images of L929 cells treated with PEG-biofunctionalized CdS, CdSe and CdTe. **a**, **d** and **g** shows the bright field images of CdS, CdSe and CdTe bio-functionalized QDs treated cells respectively. **b**, **e** and **g** shows the fluorescence of the particles and we found any particles localized in cytoplasm. **c**, **f** and **h** shows the lysotracker stain of L929 cells to show their viability. The inset in Fig. 14 f shows the bright field of L929 cells treated with lysotracker along with bio-functionalized CdSe QDs. This clearly depicts that the fluorescence has come from green fluorescent lysotracker stain and not from particle

time dependent uptake of biofunctionalized QDs (Fig. 11). However after 6 h, there was no quite higher level of QD internalization which shows that the folate mediated internalization/endocytosis has achieved saturation (Fig. 12). This clearly depicted to us that 4 h incubation is enough for the higher amount of biofunctionalized particle internalization into MCF-7 cancer cell line.

To analyze whether the cells are alive and healthy after biofunctionalized QD treatment, we have utilized DAPI (Fig. 13). The cell's nucleus was stained with DAPI to clearly depict the cell viability. The DAPI stain tracks only the viable organelle—nucleus and all the cells presented perfect DAPI staining proving that they were viable. The confocal images clearly provide evidence for the presence of nanomaterials in the cell's cytoplasm, crossing the plasma membrane of cells. The luminescence of all three biofunctionalized QDs was seen in the cytoplasm, probably entrapped in the vesicles around the nucleus. This suggests that there is no nuclear permeability of nanomaterials.

In case of normal L929 cell lines, which express low folate receptors level on plasma membrane, we observed only few targeted QDs entering them and getting endocytosed. We observed that those cells showed any proper intake of QDs by 2 h and at 4 h (Fig. 14), we observed same level of particle uptake and showed time dependency. The cells were viable and healthy confirmed by lysotracker staining but when compared to MCF-7 cancer cells, they show poor internalization of nanomaterials, which stands as an added advantage for targeted QDs.

Previous reports of biocompatibility achieved using cadmium chalcogenide QDs for biological applications are accomplished using passivation ZnS shell or silica shell over the QDs core to reduce metal ion leakage. This passivation shell reduced the luminescent property of the QDs and also requires time for processing. We have achieved excellent stable luminescence and biocompatible property with PEG biofunctionalization. The added advantage of this method is PEG functionalized QDs are able to gain decent entry to cells and are effectively endocytosed by cells within short period of time. From all the above results, we have concluded that biofunctionalized cadmium chalcogenide QDs showed increased biocompatibility and high specificity, which were essential strategies for utilization of materials for biological diagnosis.

Conclusion

In conclusion, we have shown the success of synthesizing three differently fluorescent cadmium chalcogenide QDs and PEG-lipid coating as molecular probe for optical imaging of cancer with folate targeting scheme. The in vitro results demonstrated high specificity of this contrast agent for cancer cells, suggesting its potential for detection of tumor in in vivo models and real time. Even after PEG functionalization, the nanotools retained the fluorescent properties of parental QDs. These functionalized nanoprobes showed cell specific targeting through folate receptors and the particles are internalized by folate mediated endocytosis. To summarize we believe that our differently luminescent nanoprobes would find their application in in vivo cancer targeting and other biomedical application in near future due to their superior properties of fluorescence, specificity, monodispersity, biocompatibility and smaller size for effective internalization.

Acknowledgement Aby Cheruvathoor Poulose, Srivani Veeranarayanan, M. Sheikh Mohamed and Sreejith Raveendran thank Ministry of Education, Culture, Sports, Science and Technology (MEXT), Japan for providing financial support, the Monbukagakusho fellowship. Authors thank Prof. Fukushima for Photoluminescence measurement.

References

1. Santra S, Malhotra A (2011) Fluorescent nanoparticle probes for imaging cancer. Nanomed Nanobiotechnol 3:501–510
2. ACS (2009) Cancer facts & figures. American Cancer Society, Atlanta
3. van Schoonveld MM, Cormode DP, Koole R, van Wijngaarden JT, Calcagno C, Skajaa T, Hilhorst J, Hart DCT, Fayad ZA, Mulder WJM, Meijerink A (2010) A fluorescent, paramagnetic and PEGylated gold/silica nanoparticle for MRI, CT and fluorescent imaging. Contrast Media Mol Imaging 5(4):231–236
4. Wang X, Yang L, Chen Z, Shin DM (2008) Application of nanotechnology in cancer therapy and imaging. CA Cancer J Clin 58:97–110
5. Jiang S, Gnanasammandhan MK, Zhang Y (2010) Optical imaging-guided cancer therapy with fluorescent nanoparticles. J R Soc Interface 7:3–18
6. Santra S, Dutta D, Walter GA, Moudgil BM (2005) Fluorescent nanoparticles probes for cancer imaging. Technol Cancer Res Treat 4:590–599
7. Bothun GD, Rabideau AE, Stoner MA (2009) Hepatoma cell uptake of cationic multifluorescent quantum dot liposomes. J Phys Chem B 113(22):7725–7728
8. Veeranarayanan S, Cheruvathoor AP, Mohamed S, Aravind A, Nagaoka Y, Yoshida Y, Maekawa T, Sakthi Kumar D J Fluoresc. doi:10.1007/s10895-011-0991-3
9. Mulder WJM, Cstermans K, van Beijnum JR, Oude Egbrink MGA, Chin PTK, Fayad ZA, Lowik CWGM, Kaijzel EL, Que I, Storm G, Strijkers GJ, Griffioen AW, Nicolay K (2009) Molecular imaging of tumor angiogenesis using αvβ3-integrin targeted multimodal quantum dots. Angiogenesis 12:17–24
10. Mulder WJM, Koole R, Brandwijk RJ, Storm G, Chin PTK, Strijkers GJ, de Mello Donega C, Nicolay K, Griffioen AW (2006) Quantum dots with a paramagnetic coating as bimodal molecular imaging probe. Nano Lett 6(1):1–6
11. Nahrendorf M, Jaffer FA, Kelly KA, Sosnovik DE, Aikawa E, Libby P, Weissleder R (2006) Noninvasive vascular cell adhesion molecule-1 imaging identifies inflammatory activation of cells in atherosclerosis. Circulation 114(14):1504–1511
12. Gao X, Cui Y, Levenson RM, Chung LW, Nie S (2004) In vivo cancer targeting and imaging with semiconductor quantum dots. Nat Biotechnol 22(8):969–976

13. Tong S, Hou SJ, Zheng ZL, Zhou J, Bao G (2010) Coating optimization of superparamagnetic iron oxide nanoparticles for high T_2 relaxivity. Nano Lett 10(11):4607–4613
14. Weissleder R, Mahmood U (2001) Molecular imaging. Radiology 219:316–333
15. van Tilborg GAF, Mulder WJM, Chin PTK, Storm G, Reutelingsperger CP, Nicolay K, Strijkers GJ (2006) Annexin A5-conjugated quantum dots with a paramagnetic lipidic coating for the multimodal detection of apoptopic cells. Bioconjugate Chem 17(4):865–868
16. Kamaly N, Miller AD (2010) Paramagnetic liposome nanoparticles for cellular and tumor imaging. Int J Mol Sci 11:1759–1776
17. Chen W (2008) Nanoparticle fluorescence based technology for biological applications. J Nanosci Nanotechnol 8(3):1019–1051
18. Morgan NY, English S, Chen WW, Chernomordik V, Russo A, Smith PD, Gandjbakhche A (2005) Real time in vivo non-invasive optical imaging using near-infrared fluorescent quantum dots. Acad Radiol 12:313–323
19. Dubertret B, Skourides P, Norris DJ, Nioreaux V, Brivanlou AH, Libchaber A (2002) In vivo imaging of quantum dots encapsulated in phospholipid micelles. Science 298:1759–1762
20. Wang CH, Chen CW, Wei CM, Chen YF, Lai CW, Ho ML, Chou PT (2009) Resonant energy transfer between CdSe/ZnS Type I and CdSe/ZnTe type II quantum dots. J Phys Chem C 113(35):15548–15552
21. Kuo CW, Chueh DY, Singh N, Chien FC, Chen P (2011) Targeted nuclear delivery using peptide-coated quantum dots. Bioconjugate Chem 22(6):1073–1080
22. Song EQ, Zhang ZL, Luo QY, Lu W, Shi YB, Pang DW (2009) Tumor cell targeting using folate-conjugated fluorescent quantum dots and receptor-mediated endocytosis. Clin Chem 55(5):955–963
23. Lee J, Ji K, Kim J, Park C, Lin KH, Yoon TH, Choi K (2010) Acute toxicity of two CdSe/ZnSe quantum dots with different surface coating in *Daphnia magna* under various light conditions. Environ Toxicol 25:593
24. Mulder WJM, Strijkers GJ, Nicolay K, Griffioen AW (2010) Quantum dots for multimodal imaging of angiogenesis. Angiogenesis 13:131–134
25. Tong S, Hou S, Ren B, Zheng Z, Bao G (2011) Self-assembly of phospholipid-PEG coating on nanoparticles through dual solvent exchange. Nano Lett 11(9):3720–3726
26. Al-Jamal WT, Al-Jamal KT, Tian B, Cakebread A, Halket JM, Kostarelos K (2009) Tumor targeting of functionalized quantum dot-liposome hybrids by intravenous administration. Mol Pharm 6 (2):520–530
27. Maoquan C, Zhuo S, Xu J, Sheng Q, Hou S, Wang R (2010) Liposome-coated quantum dots targeting the sentinel lymph node. J Nanopart Res 12:187–197
28. Chen CH, Yao J, Durst RA (2006) Liposome encapsulation of fluorescent nanoparticles: quantum dots and silica nanoparticles. J Nanopart Res 8:1033–1038
29. Cai W, Shin DW, Chen K, Gheysens O, Cao Q, Wang SX, Gambhir SS, Chen X (2006) Peptide-labeled near-infrared quantum dots for imaging tumor vasculature in living subjects. Nano Lett 6(4):669–676
30. Gao X, Cui Y, Levenson RM, Chung LW, Nie S (2004) In vivo cancer targeting and imaging with semiconductor quantum dots. Nat Biotechnol 22(8):969–976
31. Vila A, Gill H, McCallion O, Alonso MJ (2004) Transport of PLA-PEG particles across the nasal mucosa: effect of particle size and PEG coating density. J Contr Release 98(2):231–244
32. Zhang Y, Kohler N, Zhang M (2002) Surface modification of superparamagnetic magnetite nanoparticles and their intracellular uptake. Biomaterials 23(7):1553–1561
33. Yang H, Lou C, Xu M, Wu C, Miyoshi H, Liu Y (2011) Investigation of folate-conjugated fluorescent silica nanoparticles for targeted delivery to folate receptor-positive tumors and their internalization mechanism. J Nanomedicine 6:2023–2032
34. Zhang LW, Monteiro-Riviere NA (2009) Mechanisms of quantum dot nanoparticle cellular uptake. Toxicol Sci 110:138–155